



Sb–Sn alloy anodes for Li-ion batteries: The ternary system Li–Sb–Sn

Patric Berger, Hans Flandorfer*

University of Vienna, Faculty of Chemistry, Institute of Inorganic Chemistry – Functional Materials, Althanstraße 14, 1090, Vienna, Austria



ARTICLE INFO

Article history:

Received 29 July 2020

Received in revised form

8 September 2020

Accepted 27 September 2020

Available online 28 September 2020

Keywords:

Electrode materials

Intermetallics

Phase diagrams

X-ray diffraction

ABSTRACT

Lithium containing alloy systems are in the focus of many studies as potential electrode materials for lithium ion batteries (LiBs). However, the tremendous volume changes during the lithiation prevent a common application of these materials in nowadays used batteries. Nevertheless, the ternary Li–Sb–Sn system is considered as promising electrode material, as the binary compound $\text{Sb}_x\text{Sn}_{1-x}$ shows a relatively high rechargeable capacity. Therefore, we investigated the phase relations of this system experimentally, in order to understand the lithiation pathways during charge and discharge process.

Two isothermal sections in the Li–Sb–Sn system at 300 °C and 400 °C respectively, have been studied by 50 samples applying powder X-ray diffraction (PXRD). It has been shown, that SbSn can uptake up to 15 at.% Li, without changing the corresponding crystal structure. Beyond, the Li-rich compound Li_3Sb forms with simultaneous precipitation of liquid (Sn). The ternary phase, $\text{Li}_8\text{Sb}_x\text{Sn}_{3-x}$, earlier published by same authors, has been confirmed.

© 2020 The Authors. Published by Elsevier B.V. This is an open access article under the CC BY license (<http://creativecommons.org/licenses/by/4.0/>).

1. Introduction

The ternary system Li–Sb–Sn has recently obtained much attention in regards to the application of Sb–Sn alloys as anode material for lithium ion batteries (LiBs). In particular, the non-stoichiometric compound $\text{Sb}_x\text{Sn}_{1-x}$ has been studied in detail, for example see Ref. [1–4], and distinguished by a high rechargeable capacity of 600 mAh g^{-1} [3], in contrast to graphite with 372 mAh g^{-1} . The cycling stability of pure metal anodes like Sb or Sn is very low due to crack formation and finally pulverization caused by enormous volume expansion on alloying. Generally, several approaches to reduce the mechanical stress on lithiation are under discussion. Beside nano-texturing of the active material itself, e.g. fibrous porous SnO_2 -anodes [5], also nano-composite material like multi-wall Sn/SnO_2 @carbon hollow nanofibers [6], nano- SnO_2 encapsulated in 3D rigid porous carbon [7] and gyroid 3D networks in $\text{Si}/\text{SiO}_x/\text{C}$ [8] have been investigated. In case of metal anodes, alloys show much higher mechanical stability on cycling compared to pure elements [1].

Electrodes consisting of Sb–Sn intermetallics are conversion/formation type electrodes; Li-rich alloys are formed during the lithiation process, also compare [9,10]. The lithiation process of SbSn was reported by Trifonova et al. [3] based on XRD studies as follows:

- (a) $\text{SnSb} + 3 \text{Li}^+ + 3 \text{e}^- \rightleftharpoons \text{Li}_3\text{Sb} + \text{Sn}$
- (b) $5 \text{Sn} + 2 \text{Li}^+ + 2 \text{e}^- \rightleftharpoons \text{Li}_2\text{Sn}_5$
- (c) $\text{Li}_2\text{Sn}_5 + 3 \text{Li}^+ + 3 \text{e}^- \rightleftharpoons 5 \text{LiSn}$
- (d) $\text{LiSn} + x \text{Li}^+ + x \text{e}^- \rightleftharpoons \text{Li}_{1+x}\text{Sn}$

Thereby, the first stage of charge (a) ends up in the formation of the most stable compound Li_3Sb by a conversion reaction, accompanied by simultaneous precipitation of nano-structuring pure Sn, which absorbs mechanical strain upon lithiation. Further lithiation (reactions b–d) leads to the formation of different Li–Sn compounds, with increasing Li-content, depending on the level of charge. The most lithium-rich compound in Li–Sn is $\text{Li}_{17}\text{Sn}_4$.

The lithiation process in solid state is certainly controlled by diffusion kinetics. Nevertheless, in order to understand, control and predict lithiation pathways in such systems, the knowledge of phase equilibria, crystal structures and thermodynamic properties is highly necessary. Therefore, we investigated phase relations in the ternary Li–Sb–Sn system experimentally. The enthalpy of mixing in the liquid ternary was determined in another work [11]. Both works will provide essential thermodynamic information for CALPHAD optimization, which can be e.g., used for extrapolations to ambient temperature at which LiBs usually operate.

* Corresponding author.

E-mail address: hans.flandorfer@univie.ac.at (H. Flandorfer).

2. Literature review

2.1. Li–Sb

One of the first assessments of the binary Li–Sb system was carried out by Sangster and Pelton [12], which is especially based on earlier works done by Weppner and Huggins [13] and the assumption that liquid Li–Sb alloys have very similar behavior compared to Li–Bi alloys, for which thermodynamic data [14–16] were already available. Their phase diagram version shows two intermetallic compounds, Li_2Sb , first discovered and characterized by powder X-ray diffraction in 1974 by Ref. [17] and later by Ref. [18], as well as Li_3Sb , which was synthesized for the first time at the beginning of the 20th century by LeBeau [19] and further analyzed by Brauer und Zintl [20]. The latter authors [20] also reported two modifications for Li_3Sb , a cubic and a hexagonal structure type, with an estimated phase transformation temperature of approx. 650 °C and a melting point between 1150 and 1300 °C. Shortly thereafter, Fedorov [21] published a phase diagram including four intermetallic compounds. In addition to the already known alloys Li_3Sb and Li_2Sb , the two alloys LiSb_2 and Li_3Sb_2 were described in his work. Due to the facts, that sample preparation was done by electrolysis of a LiCl – KCl mixture with Sb as an anode and no annealing procedure was carried out, this work cannot be considered as equilibrium phase diagram, also mentioned by Ref. [9,22]. Furthermore, among others, the compounds KSb_2 and K_5Sb_4 are reported to exist [23], which could have been formed on electrolysis and erroneously interpreted as Li–Sb compounds. In the following years several groups generated a variety of assessments of thermodynamic and thermochemical data [24–27].

It was Beutl and co-workers [9], who investigated the entire system Li–Sb experimentally by means of PXRD, differential thermal analysis and drop solution calorimetry. Their phase diagram version shows only two intermetallic compounds, Li_2Sb and Li_3Sb , whereby only the hexagonal structure of Li_3Sb is stable down to room temperature. According to their investigations, the cubic modification of Li_3Sb is metastable and is first formed by the powdering process. Li_3Sb melts congruently at 1307 °C, whereas Li_2Sb is formed by a peritectic reaction at 585 °C. Additionally, two eutectic reactions ($\text{L} \rightarrow \text{Li}_2\text{Sb} + \text{Sb}$ at 471 °C and $\text{L} \rightarrow (\text{Li}) + \text{Li}_3\text{Sb}$ at 178 °C) were determined by DTA measurements. The phase diagram of Beutl et al. [9] will be accepted for our investigations. The last assessments were conducted by Li et al. [28] and Zhang et al. [29].

2.2. Li–Sn

A preliminary assessment of the binary Li–Sn system, including all relevant literature data up to this time, was done by Sangster and Bale [30] in 1998. Their phase diagram version exhibits seven Li–Sn alloys ($\text{Li}_{22}\text{Sn}_5$, Li_7Sn_2 , $\text{Li}_{13}\text{Sn}_5$, Li_5Sn_2 , Li_7Sn_3 , LiSn and Li_2Sn_5), from which only Li_7Sn_2 shows a significant homogeneity range of about 2 at.% towards the Sn-rich side. All other intermetallic compounds are drawn as line phases. While $\text{Li}_{22}\text{Sn}_5$, Li_7Sn_2 and LiSn crystallize congruently from the liquid, the other four alloys arise from peritectic reactions at given temperatures. Thermodynamic assessments are further available from Yin et al. [31], Du et al. [32] and Wang et al. [33]. Their phase diagrams exhibit similarities in their general outline, but differ by the number of intermetallic phases. While Yin et al. [31] report seven intermetallic alloys (the same as [30]), the phase diagram of Du et al. [32] and Wang et al. [33] further includes the compound Li_8Sn_3 , first described by Gasior et al. [34] and later mentioned by Giel et al. [35]. Gasior et al. [34] stated the existence of this compound solely based on a kink in coulometric titration of Sn with Li. Giel et al. [35] repeated the

coulometric titration and confirmed the appearance of the kink. However, PXRD investigations of alloys formed at concentrations of the kink did not reveal any indication of a new structure, but showed that the alloy was not in equilibrium. Up to now, this compound has never been proven or described by means of thermal analysis or crystal structure investigations.

Recently, Li et al. [10] investigated the Li–Sn system experimentally by PXRD and differential thermal analysis of 12 samples. In general, the Li–Sn system according to Li et al. [10] is in good agreement with the work of Sangster and Bale [30]. It mainly differs in the formula of the highest lithiated phase ($\text{Li}_{22}\text{Sn}_5$ now designated $\text{Li}_{17}\text{Sn}_4$, reported by Lupu et al. [36]), in slightly higher temperatures for the two peritectic reactions $\text{L} + \text{Li}_7\text{Sn}_2 \leftrightarrow \text{Li}_{13}\text{Sn}_5$ and $\text{L} + \text{Li}_5\text{Sn}_2 \leftrightarrow \text{Li}_7\text{Sn}_3$ and the conclusion, that the character of the reaction $\text{L} \leftrightarrow (\beta\text{Li}) + \text{Li}_{17}\text{Sn}_4$ (eutectic) or $\text{L} + \text{Li}_{17}\text{Sn}_4 \leftrightarrow (\beta\text{Li})$ (peritectic) is not possible. Therefore, they assumed a degenerated character of this invariant reaction. The phase diagram of Li et al. [10] will be accepted for the current work.

2.3. Sb–Sn

Phase diagram versions of the binary Sb–Sn system are quite contradictory [37–42] and were recently reviewed in a very extensive work by Schmetterer et al. [43]. Due to ambiguities in the Sb–Sn phase diagram in literature, especially concerning the crystallographic description of SbSn and the existence of a second intermetallic compound (Sb_2Sn_3), a new comprehensive experimental investigation of this system was published by the same group. Therefore, they studied the entire system with 13 alloy samples, after heat treatment with PXRD, scanning electron microscopy/energy dispersive X-ray spectroscopy (SEM/EDX) and differential thermal analysis. The new phase diagram version of Schmetterer et al. [44] exhibits two Sb–Sn alloys, SbSn , which was found being incommensurately modulated and the compound Sb_3Sn_4 with $R\bar{3}m$ space group. Conversely, the often reported phase Sb_2Sn_3 was excluded in their phase diagram version. The two stable alloys show a certain homogeneity range (SbSn : maximal extension of around 15 at.% at 326 °C; Sb_3Sn_4 : extends up to around 2.5 at.%). The maximum solubility for Sn in (Sb) was determined to be around 12.6 at.% at 425 °C, while the one for Sb in solid (Sn) is around 10 at.% at 244 °C. The peritectic reactions $\text{L}+(\text{Sb}) = \text{SbSn}$ at 425 °C, $\text{L} + \text{SbSn} = \text{Sb}_3\text{Sn}_4$ at 326 °C and $\text{L} + \text{Sb}_3\text{Sn}_4 = (\text{Sn})$ at 244 °C were fixed based on DTA measurements. The phase diagram version of Schmetterer and co-workers [44] was accepted for this work.

2.4. Li–Sb–Sn

Up to now, to the best knowledge of the authors, no information of the phase equilibria in the ternary system Li–Sb–Sn is available. Nevertheless, the compound $\text{Li}_{2.8}\text{Sn}_{0.2}\text{Sb}$ has been reported by Rönnebro et al. [45], which was supposed to be formed by the lithiation of an Ag–Sb–Sn alloy by ball milling. It was also Rönnebro et al. [46] who described in more detail the existence of ternary solubility $\text{Li}_{2+x}\text{Sn}_{1-x}\text{Sb}$ ($x \leq 1$) by performing electrochemical lithiation of $\text{Ag}_{36.4}\text{Sb}_{15.6}\text{Sn}_{48}$, together with a further ternary phase $\text{Li}_{2.6}\text{Sn}_{0.4}\text{Sb}$ within this homogeneity range. However, their analysis of powder-XRD patterns, which are naturally of low quality, is quite arbitrary. They have not measured any single crystal of this compound. Consequently, there is no clear proof for the existence of ternary phases, see also Berger et al. [47] and the discussion below. In our recent work [47] we described the ternary phase $\text{Li}_8\text{Sb}_x\text{Sn}_{3-x}$ with $0.3 \leq x \leq 1.0$, characterized by single crystal and powder X-ray diffraction. We further discussed the stereochemical and topological relations to phases in the binary sub-

systems Li–Sb and Li–Sn. In this work we showed that the crystal structures in the nearest environment of $\text{Li}_8\text{Sb}_x\text{Sn}_{3-x}$ can be assembled by the same few building blocks, for more details see also [47].

Thermodynamic data for the Li–Sb–Sn system are available from Berger and Flandorfer [11], who determined the partial and integral molar enthalpies of mixing of liquid Li–Sb–Sn alloys at 606 °C. They found a strong exothermic mixing behavior of the Li–Sb–Sn system with a minimum of $\Delta_{\text{mix}}H \approx -65 \text{ kJ mol}^{-1}$ in the binary Li–Sb system close to $x_{\text{Li}} = 0.75$. In the course of their work they further estimated the phase boundary of the liquid at 606 °C and showed that the primary formation of the high melting compound Li_3Sb dominates the solidification behavior of the entire system.

3. Experimental

3.1. Sample preparation

Sample preparation was largely done as reported recently by our group [9,10,48,49]. Pure Li, Sb and Sn or Li and Sb–Sn master alloys were the starting materials for sample preparation. Li wires (Alfa Aesar, 3.2 mm, 99.8%, with oil coating), stored in a glovebox under Ar atmosphere, tin rods (Alfa Aesar, 99.9985%) and Sb ingots (Alfa Aesar, 99.999%) were used. Initially, the oil coated Li wire was cleaned at ambient air in an ultrasonic bath in cyclohexane, followed by vacuum evaporation of the solvent. Afterwards, the thin surface oxidation layer of the lithium wire, caused by short time exposure to air, was mechanically removed inside the glovebox before use. Sb ingots were additionally purified by filtration of the liquid metal through quartz glass wool under vacuum, tin was used as purchased. Different Sb–Sn master alloys were synthesized by weighing the pure elements Sb and Sn into silica glass, followed by sealing them under vacuum. In a final step the elements were melted heating the silica ampoule with a H_2/O_2 flame. Soft shaking during the melting process provided homogenization.

Two different sample preparation techniques had to be applied because of the distinct chemical properties of the three elements. For samples with a higher Sb content and with a low Sn content, boron nitride (BN) crucibles were used since Sb reacts with Ta at elevated temperatures. Samples with higher Li contents were prepared in Ta crucibles since the vapor pressure of lithium is quite high at elevated temperatures. The detailed sample preparation by these two methods is described below:

Ta-crucible: the required amount of the elements was weight inside the glovebox and placed into Ta crucibles. These Ta crucibles were later sealed with Ta lids by arc welding under argon on a water cooled Cu mount after flushing the whole system at least three times. In some cases, the sealed crucible was transferred to an induction furnace in order to melt the elements and finally it was sealed into quartz glass ampoules under vacuum for annealing. The other part of the crucibles was first sealed in quartz glass and afterwards heated up in a muffle furnace to a maximum of 1000 °C for a few hours, before they were quenched in cold water and heated again to the annealing temperature (for details see Table 1 + 2).

BN-crucibles: the required amount of the elements was weight and placed into BN crucibles inside the glovebox. The BN crucibles themselves were closed with BN lids and finally sealed in quartz glass ampoules. The material was slowly melted and heated up to a maximum of 800 °C, quenched in cold water and finally annealed in a muffle furnace at the respective temperature for a certain time (for details see Table 1 + 2).

3.2. Powder X-ray diffraction (PXRD)

After the annealing procedure the samples were quenched in cold water and the crucibles were opened in the glovebox, for Ta crucibles a crusher was used. Pieces of the obtained samples were powdered, or rasped (for Sn-rich samples) in the glovebox and attached with dried petroleum jelly on a silicon-single crystal, which served as sample holder. For protection against oxidation during the measurement, the sample was covered by a polycarbonate cap with an O-ring tightening under Ar-atmosphere. Powder XRD measurements were conducted on a Bruker D8 diffractometer with Bragg-Brentano pseudo-focusing geometry ($\theta/2\theta$ -geometry) and $\text{CuK}\alpha$ X-radiation (40 kV/40 mA/Ni filter) using a one dimensional Si-strip detector (LynxEye detector, Bruker, Germany). Phase analysis was generally carried out by full profile Rietveld-refinement using Topas4® software supplied by Bruker, Germany.

4. Results and discussion

For constructing the isothermal sections of the Li–Sb–Sn system at 300 °C and 400 °C respectively (see Fig. 1 and Fig. 2), around 25 samples with different composition for each temperature were annealed for several weeks and investigated by PXRD. Phase analysis from all samples annealed at 300 °C and 400 °C are listed in Table 1 + 2, including all phases found, the corresponding phase fields, as well as the heat treatment conditions and the used crucibles. Detailed information about lattice parameters, obtained from Rietveld-refinement for each sample, are summarized in the supplementary data, see S1 + S2. Additionally, to draw the isothermal section the binary subsystems Li–Sb, Li–Sn and Sb–Sn of the Li–Sb–Sn system were adopted from literature (see above), including all binary alloys, their homogeneity ranges, as well as the limiting liquidus concentrations.

Experimental limitations during the investigations of the Li–Sb–Sn system, also reported by Refs. [48,49], were:

- The application of conventional metallographic methods like optical light microscope (LOM) and scanning electron microscope (SEM/EDX) was not possible. Due to the fact, that most of Li–Sb–Sn alloys are brittle and all will directly react with traces of water, embedding, grinding and polishing of such samples is extremely difficult. The direct determination of the Li-content by SEM-EDX is not possible since the yield of X-rays is too low. Additionally, the error of the determination of the Li:Sb/Sn ratio by the rest mass of Sn/Sb measurements is very high, at least $\pm 10 \text{ at.}\%$ due to the huge difference of molar masses of Li and Sb or Sn, respectively. Therefore, all ternary solubilities of unary, binary and ternary phases have been estimated, according to phase analysis and variation of lattice parameter of a high number of samples.
- A number of samples is in equilibrium with liquid phase at the respective annealing temperature. Therefore, after quenching, solidification phases were found, which are not part of the phase equilibria at the corresponding temperature. A critical assessment, considering especially the binary sub-systems Li–Sb, Li–Sn and Sb–Sn, enables the construction of the corresponding phase relations.
- Selective preparation of ternary samples in Ta-crucibles within the very narrow three phase fields, starting from the Li–Sn binary two phase equilibria at $x_{\text{Li}} = 0.7-0.77$, was almost impossible, considering the deviations from the nominal compositions of $\pm 1 \text{ at.}\%$ according to Ref. [49]. Therefore, three phase fields in this region were drawn with dashed lines in most cases.

Table 1
Samples annealed at 300 °C and their heat treatment condition as well as identified phases.

| No. | Li [at.%] | Sb [at.%] | Sn [at.%] | Melting procedure | Heat treatment [°C/ days] | Identified phases | Corresponding phase field | Crucible used | Comments |
|-----|--------------|--------------|--------------|----------------------|------------------------------|--|---|------------------|---|
| 1* | 80 | 10 | 10 | I | 300/34 | h-Li ₃ Sb, Li ₁₇ Sn ₄ | Li + Li ₃ Sb + Li ₁₇ Sn ₄ | Ta | Li hardly visible in XRD*** |
| 2* | 78 | 11 | 11 | I | 300/35 | h-Li ₃ Sb, Li ₁₇ Sn ₄ | Li ₃ Sb + Li ₁₇ Sn ₄ | Ta | Composition slightly shifted from nominal |
| 3 | 78 | 5 | 17 | M | 300/30 | h-Li ₃ Sb, Li ₇ Sn ₂ | Li ₃ Sb + Li ₇ Sn ₂ | Ta | Composition slightly shifted from nominal |
| 4 | 75 | 1.5 | 23.5 | I | 300/61 | Li ₇ Sn ₂ , Li ₁₃ Sn ₅ , Sn, T1 | Li ₇ Sn ₂ + Li ₁₃ Sn ₅ + T1 | Ta | Minor hydrolysis during XRD measurement (Sn) |
| 5 | 75 | 2.5 | 22.5 | M | 300/40 | h-Li ₃ Sb**, Li ₇ Sn ₂ , Sn, T1 | Li ₃ Sb + Li ₇ Sn ₂ + T1 | Ta | Minor hydrolysis during XRD measurement (Sn) |
| 6 | 75 | 8 | 17 | M | 300/31 | h-Li ₃ Sb, Li ₇ Sn ₂ , T1 | Li ₃ Sb + Li ₇ Sn ₂ + T1 | Ta | — |
| 7* | 75 | 12.5 | 12.5 | I | 300/41 | h-Li ₃ Sb, T1 | Li ₃ Sb + T1 | Ta | Composition slightly shifted from nominal |
| 8* | 73 | 5 | 22 | M | 300/48 | h-Li ₃ Sb, Li ₁₃ Sn ₅ , T1 | Li ₃ Sb + Li ₁₃ Sn ₅ + T1 | Ta | — |
| 9* | 67.5 | 30 | 2.5 | M | 300/24 | h-Li ₃ Sb, Li ₂ Sb, SbSn, Sb | Li ₃ Sb + Li ₂ Sb + SbSn | Ta | Minor hydrolysis during XRD measurement (Sb) |
| 10 | 60 | 5 | 35 | I | 300/87 | c-Li ₃ Sb**, h-Li ₃ Sb, Li ₇ Sn ₃ , LiSn | Li ₃ Sb + Li ₇ Sn ₃ + LiSn | Ta | — |
| 11* | 60 | 20 | 20 | I | 300/48 | c-Li ₃ Sb, h-Li ₃ Sb, SbSn, Sn | Li ₃ Sb + SbSn + L | Ta | — |
| 12* | 54 | 9 | 37 | M | 300/35 | c-Li ₃ Sb, h-Li ₃ Sb, LiSn, Li ₂ Sn ₅ , Sb**, Sn | Li ₃ Sb + LiSn + Li ₂ Sn ₅ | Ta | Minor hydrolysis during XRD measurement (Sb,Sn) |
| 13 | 45 | 15 | 40 | I | 300/120 | c-Li ₃ Sb, SbSn, Sn | Li ₃ Sb + SbSn + L | Ta | — |
| 14* | 40 | 30 | 30 | I | 300/60 | c-Li ₃ Sb, SbSn, Sn | Li ₃ Sb + SbSn + L | Ta | — |
| 15 | 35 | 30 | 35 | M | 300/60 | c-Li ₃ Sb, SbSn, Sn | Li ₃ Sb + SbSn + L | Ta | — |
| 16* | 30 | 35 | 35 | M | 300/60 | c-Li ₃ Sb, Sb**, SbSn, Sn | Li ₃ Sb + SbSn + L | Ta | Minor hydrolysis during XRD measurement (Sb) |
| 17 | 30 | 40 | 30 | M | 300/27 | c-Li ₃ Sb, SbSn, Sb** | Li ₃ Sb + SbSn | Ta | Minor hydrolysis during XRD measurement (Sb) |
| 18 | 30 | 45 | 25 | M | 300/31 | Li ₂ Sb, Sb, SbSn | Li ₂ Sb + Sb + SbSn | BN | — |
| 19 | 30 | 50 | 20 | M | 300/23 | Li ₂ Sb, Sb, SbSn | Li ₂ Sb + Sb + SbSn | BN | — |
| 20 | 20 | 5 | 75 | I | 300/37 | c-Li ₃ Sb**, SbSn**, Sn | Li ₃ Sb + SbSn + L | Ta | — |
| 21 | 20 | 27 | 53 | I | 300/28 | c-Li ₃ Sb, SbSn, Sn | Li ₃ Sb + SbSn + L | Ta | — |
| 22 | 20 | 76 | 4 | M | 300/23 | Sb, Li ₂ Sb | Li ₂ Sb + Sb | BN | — |
| 23* | 16 | 16.8 | 67.2 | M | 300/56 | c-Li ₃ Sb**, SbSn, Sn, Ta**** | Li ₃ Sb + SbSn + L | Ta | — |
| 24* | 14 | 17 | 69 | M | 300/23 | SbSn, Sn | SbSn + L | Ta | — |
| 25 | 10 | 46.8 | 43.2 | I | 300/22 | SbSn | SbSn | Ta | — |
| 26* | 10 | 67.5 | 22.5 | M | 300/53 | Li ₂ Sb, Sb, SbSn | Li ₂ Sb + Sb + SbSn | BN | — |
| 27 | 5 | 65 | 30 | I | 300/28 | Sb, SbSn | Sb + SbSn | Ta | — |

* = Samples were prepared with Sb–Sn master alloys.

** = only traces were observed.

*** = Li has only three electrons and therefore a very low scattering power for X-rays. Thus its detections is only possible with long exposure time. However, diffraction intensities from phases which contain larger amounts of Sb/Sn (quite high scattering power) would lead to an overflow of the detector at the same time.

**** = from the crucible wall.

I = induction furnace.

M = muffle furnace.

- It is known from literature [9], that the *cubic* modification of Li₃Sb is a meta-stable phase, being stress-stabilized, e.g. on powdering, observed by Beutl and Flandorfer [49], during their investigations in the Li–Sb and Cu–Li–Sb system. Thus, in the three phase field Li₃Sb + SbSn + L, both modifications, the hexagonal and the cubic type of Li₃Sb, were found in the same samples. With decreasing Li amount and increasing Sn amount, the cubic modification occurs even solely, what of course can be attributed to the fact, that Li-poor and at the same time Sn-rich samples are ductile and rather greasy and therefore, more power is necessary for powdering. On the other hand, in samples upon 60 at.%, Li where brittle Li–Sn phases are in equilibrium with Li₃Sb, only its hexagonal modification was found. We have already discussed the occurrence of a ternary compound Li_{2.8}Sn_{0.2}Sb stated by Rönnebro et al. [45,46]. It shows the same structure as cubic Li₃Sb (BiF₃-type) and is a member of the ternary solubility of Sn into Li₃Sb, according to Li_{2+x}Sn_{1-x}Sb with $x \leq 1$, claimed by the authors; in Ref. [46] they report a further compound within this solubility range, Li_{2.6}Sn_{0.4}Sb, which corresponds to $x = 0.6$, or 10 at.% Sn. They derived those compositions from Rietveld refinements of powder patterns, allowing

Sn occupation at the 8c Li-sites. However, their XRD patterns were recorded on multi-phase samples after mechanical alloying [45] or electrochemical lithiation [46]. We doubt that the results are significant regarding 1) the poor quality of the multi-phase patterns, 2) the large difference of electron numbers of Li and Sn, 3) a solubility of 10 at.% Sn in Li₃Sb can be excluded by our investigations and 4) that there is no systematic change of lattice parameters of the cubic Li₃Sb structure throughout the solubility range. We rather think that only stress-induced cubic Li₃Sb [9] was present in the samples. Nevertheless, the existence of a real ternary phase, which was stabilized by small additions of Sn to the metastable cubic Li₃Sb, cannot be totally excluded.

- Impurities of Sb, as well as Sn, were sometimes observed especially in Li-rich samples. We assume that this observation is caused by little hydrolysis of the Li–Sb and Li–Sn phases, respectively during the XRD measurements (measurement time for each sample was usually 2 h), although a polymer cap and dry petroleum jelly was used and preparation was done in a glovebox under argon atmosphere. The reaction products of hydrolysis are Li(OH) and Sn/Sb, whereas the first cannot be detected by PXRD since it has such a low scattering power.

Table 2

Samples annealed at 400 °C and their heat treatment condition as well as identified phases.

| No. | Li [at.%] | Sb [at.%] | Sn [at.%] | Melting procedure | Heat treatment [°C/days] | Identified phases | Corresponding phase field | Crucible used | Comments |
|-----|--------------|--------------|--------------|-----------------------|-----------------------------|---|---|------------------|---|
| 1* | 80 | 10 | 10 | M | 400/20 | h-Li ₃ Sb, Li ₁₇ Sn ₄ | Li + Li ₃ Sb + Li ₁₇ Sn ₄ | Ta | Li hardly visible in XRD*** |
| 2* | 80 | 15 | 5 | I | 400/50 | h-Li ₃ Sb, Li ₁₇ Sn ₄ | Li + Li ₃ Sb + Li ₁₇ Sn ₄ | Ta | Li hardly visible in XRD*** |
| 3 | 75 | 5 | 20 | directly to 400 °C | 400/29 | h-Li ₃ Sb, Li ₇ Sn ₂ , T1 | Li ₃ Sb + Li ₇ Sn ₂ + T1 | Ta | — |
| 4* | 75 | 12.5 | 12.5 | M | 400/92 | h-Li ₃ Sb, T1 | Li ₃ Sb + T1 | Ta | Composition slightly shifted from nominal |
| 5 | 70 | 5 | 25 | I | 400/35 | h-Li ₃ Sb, Li ₇ Sn ₃ , LiSn, Sb**, Sn | Li ₃ Sb + Li ₇ Sn ₃ + LiSn | Ta | Minor hydrolysis during XRD measurement (Sb, Sn) |
| 6 | 65 | 5 | 30 | M | 400/38 | h-Li ₃ Sb, Li ₇ Sn ₃ , LiSn, Sb**, Sn | Li ₃ Sb + Li ₇ Sn ₃ + LiSn | Ta | Minor hydrolysis during XRD measurement (Sb, Sn) |
| 7* | 60 | 20 | 20 | M | 400/99 | h-Li ₃ Sb, c-Li ₃ Sb, SbSn, Sb, Sn | Li ₃ Sb + SbSn + L | Ta | Minor hydrolysis during XRD measurement (Sb) |
| 8 | 55 | 5 | 40 | I | 400/35 | h-Li ₃ Sb, c-Li ₃ Sb, LiSn, Li ₂ Sn ₅ , Sn** | Li ₃ Sb + LiSn + L | Ta | Li ₂ Sn ₅ formed during quenching of L; Composition slightly shifted from nominal |
| 9* | 50 | 37.5 | 12.5 | I | 400/34 | c-Li ₃ Sb, Li ₂ Sb, SbSn, Sb** | Li ₃ Sb + Li ₂ Sb + SbSn | Ta | Minor hydrolysis during XRD measurement (Sb) |
| 10 | 44 | 16 | 40 | M | 400/37 | c-Li ₃ Sb, h-Li ₃ Sb, SbSn, Sn, Sb | Li ₃ Sb + SbSn + L | Ta | Minor hydrolysis during XRD measurement (Sb) |
| 11 | 40 | 30 | 30 | M | 400/45 | c-Li ₃ Sb, SbSn, Sn | Li ₃ Sb + SbSn + L | Ta | — |
| 12* | 40 | 45 | 15 | I | 400/34 | Li ₂ Sb, Sb, SbSn | Li ₂ Sb + Sb + SbSn | BN | — |
| 13 | 35 | 5 | 60 | M | 400/34 | c-Li ₃ Sb**, Li ₂ Sn ₅ , Sn | Li ₃ Sb + L | Ta | Li ₂ Sn ₅ formed during quenching of L |
| 14 | 30 | 5 | 65 | M | 400/38 | c-Li ₃ Sb, h-Li ₃ Sb, Li ₂ Sn ₅ , Sn | Li ₃ Sb + L | Ta | Li ₂ Sn ₅ formed during quenching of L |
| 15 | 25 | 45 | 30 | M | 400/34 | c-Li ₃ Sb, SbSn, Sb ₂ Ta | Li ₃ Sb + SbSn | Ta | Sb ₂ Ta due to reaction of Sb with Ta-crucible |
| 16 | 20 | 20 | 60 | M | 400/45 | c-Li ₃ Sb**, SbSn, Sn | Li ₃ Sb + SbSn + L | Ta | — |
| 17 | 20 | 45 | 35 | M | 400/34 | c-Li ₃ Sb, SbSn, Sb ₂ Ta, Sn** | Li ₃ Sb + SbSn + L | Ta | Sb ₂ Ta due to reaction of Sb with Ta-crucible; Sb content lower than nominal |
| 18 | 20 | 76 | 4 | M | 400/61 | Li ₂ Sb, Sb | Li ₂ Sb + Sb | BN | — |
| 19* | 15 | 42.5 | 42.5 | M | 400/49 | c-Li ₃ Sb, SbSn, Sn | Li ₃ Sb + SbSn + L | Ta | — |
| 20 | 10 | 20 | 70 | M | 400/31 | c-Li ₃ Sb**, SbSn, Sb**, Sn | SbSn + L | Ta | Li ₃ Sb formed during quenching of L; Minor hydrolysis during XRD measurement (Sb) |
| 21* | 10 | 45 | 45 | M | 400/38 | c-Li ₃ Sb**, SbSn, Sn, Sb ₂ Ta | Li ₃ Sb + SbSn + L | Ta | Sb ₂ Ta due to reaction of Sb with Ta-crucible |
| 22* | 5 | 47.5 | 47.5 | M | 400/49 | SbSn, Sn** | SbSn + L | Ta | — |
| 23* | 5 | 71.3 | 23.8 | M | 400/34 | Sb, SbSn | Sb + SbSn | Ta | — |

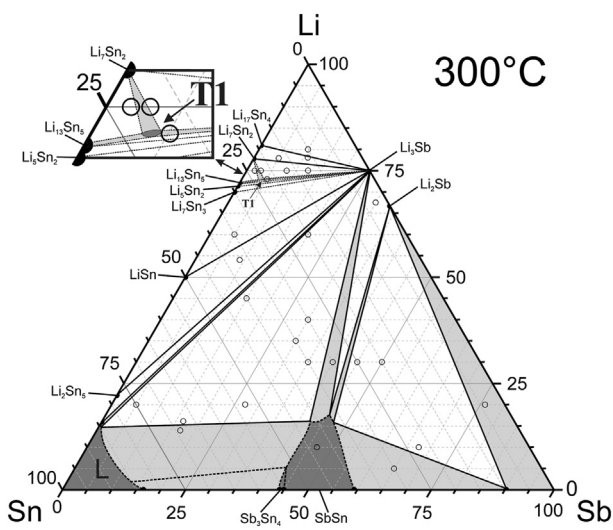
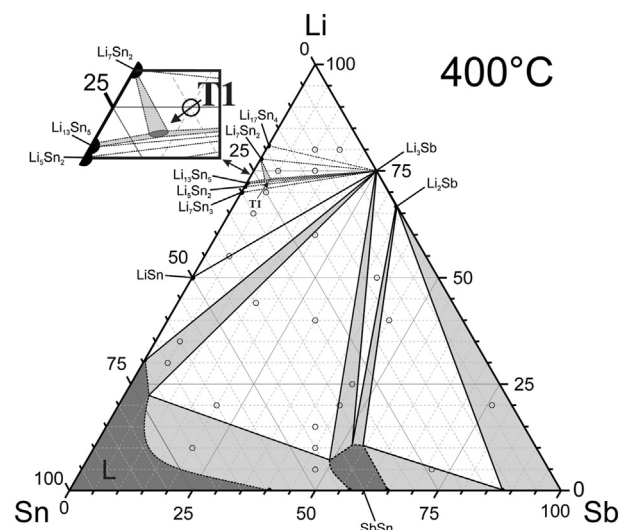
* = Samples were prepared with Sb–Sn master alloys.

** = only traces were observed.

*** = Li has only three electrons and therefore a very low scattering power for X-rays. Thus its detection is only possible with long exposure time. However, diffraction intensities from phases which contain larger amounts of Sb/Sn (quite high scattering power) would lead to an overflow of the detector at the same time.

I = induction furnace.

M = muffle furnace.

**Fig. 1.** Isothermal section at 300 °C with annealed samples, indicated as unfilled circles. Estimated phase equilibria are drawn with dashed lines. Single, two- and three-phase equilibria are drawn in dark-grey, light-grey and white, respectively.**Fig. 2.** Isothermal section at 400 °C with annealed samples, indicated as unfilled circles. Estimated phase equilibria are drawn with dashed lines. Single, two- and three-phase equilibria are drawn in dark-grey, light-grey and white, respectively.

Both isothermal sections exhibit similarities in their general outline, but differ i) in the number of three-phase equilibria, ii) in the number of intermetallic phases and iii) in the elongation of the homogeneity ranges of the liquid phase and SbSn. In general, $\text{Li}_8\text{Sb}_x\text{Sn}_{3-x}$ [47], indicated as T1 throughout this work, was the only ternary compound found during our investigations. The existence of this phase was confirmed by the corresponding three-phase equilibria, compare Fig. 1 + 2. Especially in this area of the isothermal sections, the three phase equilibria are rather narrow and therefore investigations were quite difficult. All five three-phase equilibria in this part of the phase diagram include the binary phase Li_3Sb , except the three phase field $\text{Li}_7\text{Sn}_2 + \text{Li}_{13}\text{Sn}_5 + \text{T1}$. Samples which were placed into the three phase field $\text{Li} + \text{Li}_3\text{Sb} + \text{Li}_{17}\text{Sn}_4$ only exhibit $\text{Li}_{17}\text{Sn}_4$ and Li_3Sb in XRD analysis. Nevertheless, these three alloys are supposed to form this three-phase equilibrium, since pure Li cannot be detected together with the other two phases by PXRD measurements, due to the large difference of the scattering factors between Li and Sb/Sn.

In the Li-poor region the isothermal sections at 300 °C and 400 °C particularly differ in the appearance of Sb_3Sn_4 and Li_2Sn_5 , which are not stable anymore at 400 °C. Thus, the corresponding three phase fields $\text{L} + \text{SbSn}/\text{Sb}_3\text{Sn}_4$ (see below), $\text{L} + \text{Li}_3\text{Sb} + \text{Li}_2\text{Sn}_5$ and $\text{Li}_3\text{Sb} + \text{Li}_2\text{Sn}_5 + \text{LiSn}$ are not present at 400 °C. The expansion of the liquid and the solubility of Sn into Sb rises with temperature whereas the solubility of Li into SbSn lowers. The expansion of the liquid, as well as the expansion of SbSn, were estimated based on adjacent phase fields.

Since the two-phase field $\text{SbSn} + \text{Sb}_3\text{Sn}_4$ was considered to be very small in Sb–Sn by Schmetterer et al. [44], the three phase field $\text{L} + \text{SbSn} + \text{Sb}_3\text{Sn}_4$ was estimated to be also very small and is thus indicated with a dashed line. The three-phase equilibrium $\text{L} + \text{Li}_3\text{Sb} + \text{LiSn}$ forms only at 400 °C. The three other three-phase equilibria ($\text{Sb} + \text{Li}_2\text{Sb} + \text{SbSn}$, $\text{SbSn} + \text{Li}_2\text{Sb} + \text{Li}_3\text{Sb}$ and $\text{L} + \text{SbSn} + \text{Li}_3\text{Sb}$) are present in both isothermal sections but differ in their limiting concentrations. We have set three samples in the three-phase field ($\text{Sb} + \text{Li}_2\text{Sb} + \text{SbSn}$), No. 18, 19 and 26 at 300 °C. It has to be noted that the equilibrium phase (Sb) in sample No. 18 rather shows lattice parameters ($a = 4.3013 \text{ \AA}$, $c = 11.2775 \text{ \AA}$) similar to pure Sb ($a = 4.301 \text{ \AA}$, $c = 11.232 \text{ \AA}$) [50] than those for (Sb), with 10 at.% Sn solved, in samples No. 19 ($a = 4.2650 \text{ \AA}$, $c = 11.4567 \text{ \AA}$) and 26 ($a = 4.2663 \text{ \AA}$, $c = 11.4449 \text{ \AA}$); see Fig. 1 and S1. This is probably due to a coring effects which is also indicated by relatively large peak widths in sample No. 18 compared to 19 and 26.

It has been shown that in particular Li_3Sb from the binary Li–Sb system dominates both isothermal sections. Beside the three three-phase fields $\text{Li}_2\text{Sb} + (\text{Sb}) + \text{SbSn}$, $\text{L} + \text{SbSn}/\text{Sb}_3\text{Sn}_4$, and $\text{Li}_7\text{Sn}_2 + \text{Li}_{13}\text{Sn}_5 + \text{T1}$ all other three-phase equilibria include the binary phase Li_3Sb . A solid solubility of Li into SbSn up to 15 at.% was observed, which definitely is an important outcome, considering the studies of SbSn as new anode material for lithium-ion batteries. Indeed, according to Besenhard et al. [2], the coulometric titration of polycrystalline SbSn with Li at room temperature shows a continuous decrease of the potential which indicates a single phase process.

5. Conclusions

In the ternary system Li–Sb–Sn only one ternary compound occurs, $\text{Li}_8\text{Sb}_x\text{Sn}_{3-x}$, which was found in both isothermal sections. In general, both isothermal sections are similar in their general outline and actually, only differ by the variation of the binary systems with temperature. Our results show that lithiation of the binary phase $\text{Sb}_x\text{Sn}_{1-x}$ starts with an alloying reaction (up to 15 at.% Li at 300 °C), without changing the corresponding crystal structure.

Since the solubility of Li seems to be retrograde, it can be expected that it exists also at ambient temperature. Further lithiation leads to a conversion reaction with the formation of Li_3Sb and simultaneous precipitation of small (Sn)-crystals [3]. Ductile, micro-structured (Sn) acts as a “buffer” for mechanical stress caused by the formation of various Li–Sb and Li–Sn compounds. Only upon a Li concentration of approx. 60 at.% also Li–Sn alloys start to form. Our investigations were performed on alloys annealed at 300 °C and 400 °C, although knowledge of phase relations at lower temperatures, at which LIBs usually operate, is crucial. It has to be noted that phase equilibria at room temperature are not experimentally accessible by liquid alloying at high temperatures. This especially applies to Li–Sb–Sn where primary crystallization of Li_3Sb is dominant. Nevertheless, a reliable extrapolation to ambient temperature is possible, if measured thermodynamic data, recently published by the same authors [11], and phase diagram data from the current work are consolidated in a CALPHAD optimization. In this way the prediction of the reaction pathway during the lithiation at room temperature using SbSn as anode material would be possible. Future large scale applications of SbSn-anodes in galvanic cells are limited by relatively high costs of the materials and the discussion of declaring Sb as a toxic material which has to be largely banned from industrial productions. However, they are still interesting as niche products for special applications.

CRedit authorship contribution statement

Patric Berger: Investigation, Validation, Visualization, Writing - original draft. **Hans Flandorfer:** Conceptualization, Validation, Writing - review & editing, Supervision, Project administration, Funding acquisition.

Declaration of competing interest

The authors declare that they have no known competing financial interests or personal relationships that could have appeared to influence the work reported in this paper.

Acknowledgments

This work was supported by the DFG project FL-730/1–2 within the priority program SPP 1473, “WeNDeLIB”. We thank P. Wibner and J. Polt for doing preliminary experiments and their contributions to sample preparation. Furthermore, we thank our colleague G. Reisinger for the fruitful discussions.

Appendix A. Supplementary data

Supplementary data to this article can be found online at <https://doi.org/10.1016/j.jallcom.2020.157381>.

References

- [1] M. Winter, J.O. Besenhard, Electrochemical lithiation of tin and tin-based intermetallics and composites, *Electrochim. Acta* 45 (1999) 31–50.
- [2] J.O. Besenhard, M. Wachtler, M. Winter, R. Andreas, I. Rom, W. Sitte, Kinetics of Li insertion into polycrystalline and nanocrystalline ‘SnSb’ alloys investigated by transient and steady state techniques, *J. Power Sources* 81 (1999) 268–272.
- [3] A. Trifonova, M. Wachtler, M. Winter, J.O. Besenhard, Sn–Sb and Sn–Bi alloys as anode materials for lithium-ion batteries, *Ionics* 8 (2002) 321–328.
- [4] A.T. Tesfaye, Y.D. Yucel, M.K.S. Barr, L. Santinacci, F. Vacandio, F. Dumur, S. Maria, L. Monconduit, T. Djenizian, The electrochemical behavior of SnSb as an anode for Li-ion batteries studied by electrochemical impedance spectroscopy and electron microscopy, *Electrochim. Acta* 256 (2017) 155–161.
- [5] S.M. Hwang, Y.G. Lim, J.G. Kim, Y.U. Heo, J.H. Lim, Y. Yamauchi, M.S. Park, Y.J. Kim, S.X. Dou, J.H. Kim, A case study on fibrous porous SnO_2 anode for robust, high-capacity lithium-ion batteries, *Nanomater. Energy* 10 (2014)

- 53–62.
- [6] S.W. Gao, N. Wang, S. Li, D.M. Li, Z.M. Cui, G.C. Yue, J.C. Liu, X.X. Zhao, L. Jiang, Y. Zhao, A multi-wall Sn/SnO₂@carbon hollow nanofiber anode material for high-rate and long-life lithium-ion batteries, *Angew. Chem. Int. Ed.* 59 (2020) 2465–2472.
 - [7] H.R. Xue, J.Q. Zhao, J. Tang, H. Gong, P. He, H.S. Zhou, Y. Yamauchi, J.P. He, High-loading nano-SnO₂ encapsulated in situ in three-dimensional rigid porous carbon for superior lithium-ion batteries, *Chem. Eur. J.* 22 (2016) 4915–4923.
 - [8] J. Lee, J. Moon, S.A. Han, J. Kim, V. Malgras, Y.U. Heo, H. Kim, S.M. Lee, H.K. Liu, S.X. Dou, Y. Yamauchi, M.S. Park, J.H. Kim, Everlasting living and breathing gyroid 3D network in Si@SiO_x/C nanoarchitecture for lithium ion battery, *ACS Nano* 13 (2019) 9607–9619.
 - [9] A. Beutl, D. Cupid, H. Flandorfer, The Li-Sb phase diagram part I: new experimental results, *J. Alloys Compd.* 695 (2017) 1052–1060.
 - [10] D. Li, S. Fürtauer, H. Flandorfer, D.M. Cupid, Thermodynamic assessment and experimental investigation of the Li-Sn system, *Calphad* 47 (2014) 181–195.
 - [11] P. Berger, H. Flandorfer, Enthalpy of mixing of liquid Li-Sb-Sn alloys, *J. Mol. Liq.* 298 (2020).
 - [12] J. Sangster, A.D. Pelton, The Li-Sb (lithium-antimony) system, *J. Phase Equil.* 14 (1993) 514–517.
 - [13] W. Weppner, R.A. Huggins, Thermodynamic properties of intermetallic systems lithium-antimony and lithium-bismuth, *J. Electrochem. Soc.* 125 (1978) 7–14.
 - [14] M.A.I. Demidov, Thermodynamic properties of liquid Bi-Li alloys, *Sov. Electrochem.* 9 (1973) 1321–1322.
 - [15] B. Predel, G. Oehme, Calorimetric investigation of liquid Li-Tl, Li-Ln, and Li-Bi alloys, *Z. Metallkd.* 70 (1979) 618–623.
 - [16] M.S. Foster, S.E. Wood, C.E. Crouthamel, Thermodynamics of binary alloys. I. lithium-bismuth system, *Inorg. Chem.* 3 (1964) 1428–1431.
 - [17] R. Gerardin, J. Aubry, Préparation et identification d'un nouveau composé binaire Li₂Sb, *C. R. Acad. Sc. Paris Série C* 278 (1974) 1097–1098.
 - [18] W. Müller, Preparation and crystal-structure of Li₂Sb, *Z. Naturforsch. B Chem. Sci.* 32 (1977) 357–359.
 - [19] P. LeBeau, Sur L'antimoine de lithium et sur la preparation de quelques alliages de ce metal, *C. R. Hebd. Seances Acad. Sci.* 134 (1902) 231–233.
 - [20] G. Brauer, E. Zintl, Constitution of phosphides, arsenides, antimonides, and bismuthides of Li, Na and K, *Z. Phys. Chem.* 37 (1937) 323–352.
 - [21] P. Fedorov, Lithium-antimony system, *Russ. J. Inorg. Chem.* 40 (1995) 815–817.
 - [22] H. Okamoto, Li-Sb (lithium-antimony), *J. Phase Equil.* 17 (1996), 271–271.
 - [23] F.W. Dorn, W. Klemm, Das Verhalten der Alkalimetalle zu Halbmetallen. 5. Die Systeme des Antimons mit Kalium, Rubidium und Caesium, *Z. Anorg. Allg. Chem.* 309 (1961) 189–203.
 - [24] A.G. Morachevskii, Thermodynamic analysis of alloys of the lithium-antimony system, *Russ. J. Appl. Chem.* 75 (2002) 367–369.
 - [25] M.E. Schlesinger, Thermodynamic properties of solid binary antimonides, *Chem. Rev.* 113 (2013) 8066–8092.
 - [26] M.M. Kane, J.M. Newhouse, D.R. Sadoway, Electrochemical determination of the thermodynamic properties of lithium-antimony alloys, *J. Electrochem. Soc.* 162 (2015) A421–A425.
 - [27] A.G. Morachevskii, Lithium-antimony alloys: phase diagram, thermodynamic properties, electrochemical behavior in molten and nonaqueous electrolytes, and use in lithium-ion batteries, *Russ. J. Appl. Chem.* 88 (2015) 1737–1749.
 - [28] D. Li, A. Beutl, H. Flandorfer, D.M. Cupid, The Li-Sb phase diagram part II: calorimetry and thermodynamic assessment, *J. Alloys Compd.* 701 (2017) 186–199.
 - [29] F. Zhang, S.H. Liu, J.C. Wang, Y. Du, L.X. Sun, Experimental investigation and thermodynamic assessment of the Li-Sb system, *Calphad* 57 (2017) 28–36.
 - [30] J. Sangster, C.W. Bale, The Li-Sn (lithium-tin) system, *J. Phase Equil.* 19 (1998) 70–75.
 - [31] F. Yin, X. Su, Z. Li, J. Wang, Thermodynamic assessment of the Li-Sn (lithium-tin) system, *J. Alloys Compd.* 393 (2005) 105–108.
 - [32] Z.M. Du, Z.Q. Jiang, C.P. Guo, Thermodynamic optimizing of the Li-Sn system, *Z. Metallkd.* 97 (2006) 10–16.
 - [33] J. Wang, J. Han, I.H. Jung, D. Bairos, P. Chartrand, Thermodynamic optimizations on the binary Li-Sn system and ternary Mg-Sn-Li system, *Calphad* 47 (2014) 100–113.
 - [34] W. Gasior, Z. Moser, W. Zakulski, Thermodynamic studies and the phase diagram of the Li-Sn system, *J. Non-Cryst. Solids* 205–207 (1996) 379–382.
 - [35] H. Giel, D. Henriques, T. Markus, Investigations of the Li₈Sn₃ phase in the binary Li-Sn system using an improved coulometric-titration setup, *J. Electrochem. Soc.* 164 (2017) A907–A911.
 - [36] C. Lupu, J.G. Mao, J.W. Rabalais, A.M. Guloy, J.W. Richardson, X-ray and neutron diffraction studies on "Li_{4.4}Sn, *Inorg. Chem.* 42 (2003) 3765–3771.
 - [37] S.W. Chen, C.C. Chen, W. Gierlotka, A.R. Zi, P.Y. Chen, H.J. Wu, Phase equilibria of the Sn-Sb binary system, *J. Electron. Mater.* 37 (2008) 992–1002.
 - [38] M. Hansen, K. Anderko, Constitution of Binary Alloys, 2 ed., McGraw-Hill, New York, 1958.
 - [39] T.B. Massalski, H. Okamoto, Binary Alloy Phase Diagrams, second ed., ASM International, Materials Park, Ohio, 1990.
 - [40] H. Okamoto, Sb-Sn (antimony-tin), *J. Phase Equil.* 19 (1998) 292–292.
 - [41] B. Predel, W. Schwermann, Constitution and thermodynamics of antimony-tin System, *J. I. Met.* 99 (1971) 169–172.
 - [42] V. Vassiliev, M. Lelaurain, J. Hertz, A new proposal for the binary (Sn,Sb) phase diagram and its thermodynamic properties based on a new emf study, *J. Alloys Compd.* 247 (1997) 223–233.
 - [43] C. Schmetterer, J. Polt, H. Flandorfer, The phase equilibria in the Sb-Sn system - Part I: literature review, *J. Alloys Compd.* 728 (2017) 497–505.
 - [44] C. Schmetterer, J. Polt, H. Flandorfer, The phase equilibria in the Sb-Sn system - Part II: experimental results, *J. Alloys Compd.* 743 (2018) 523–536.
 - [45] E. Rönnebro, J.T. Yin, A. Kitano, M. Wada, T. Sakai, Comparative studies of mechanical and electrochemical lithiation of intermetallic nanocomposite alloys for anode materials in Li-ion batteries, *Solid State Ionics* 176 (2005) 2749–2757.
 - [46] E. Rönnebro, J.T. Yin, A. Kitano, M. Wada, S. Tanase, T. Sakai, Reaction mechanism of a Ag_{36.4}Sb_{15.6}Sn₄₈ nanocomposite electrode for advanced Li-ion batteries, *J. Electrochem. Soc.* 152 (2005) A152–A157.
 - [47] P. Berger, C. Schmetterer, H.S. Effenberger, H. Flandorfer, The ternary phase Li₈Sb_xSn_{3-x} with 0.3 ≤ x ≤ 1.0, *Z. Krist.-Cryst. Mater.* 235 (2020) 183–192.
 - [48] S. Fürtauer, H. Flandorfer, The Cu-Li-Sn phase diagram: isothermal sections, *J. Alloys Compd.* 682 (2016) 713–722.
 - [49] A. Beutl, H. Flandorfer, The Cu-Li-Sb system: a thermodynamic investigation on a materials system promising for lithium ion batteries, *J. Alloys Compd.* 757 (2018) 310–323.
 - [50] C.S. Barrett, P. Cucka, K. Haefner, Crystal structure of antimony at 4.2, 78 and 298°K, *Acta Crystallogr.* 16 (1963) 451–453.